


Settling of nonuniform cylinders at intermediate Reynolds numbers

Brandon R. Angle

*Department of Mechanical Engineering, Pennsylvania State University,
University Park, Pennsylvania 16802, USA*

Matthew J. Rau 

*Department of Mechanical Engineering, George Washington University, Washington, DC 20052, USA
and Department of Mechanical Engineering, Pennsylvania State University,
University Park, Pennsylvania 16802, USA*

Margaret L. Byron *

*Department of Mechanical Engineering, Pennsylvania State University,
University Park, Pennsylvania 16802, USA*



(Received 14 July 2023; accepted 10 May 2024; published 3 July 2024)

Many natural and industrial processes involve the sedimentation of nonspherical particles. Many of these particles do not have uniform mass distributions; two cases of interest are aggregates (which may be composed of multiple materials) and microplastic pollutants (which may experience localized fouling or degradation). For such particles, the centers of mass and buoyancy are not collocated. This leads to interesting settling dynamics, particularly at transition points near the onset of wake instabilities. We investigated the orientation and terminal velocity of initially horizontal, freely falling cylinders, in which the mass distribution was either constant (uniform density) or bipartite, undergoing a step change halfway along the length (compound density). Cylinders had low aspect ratios ($1 \leq AR \leq 4$) and fell at intermediate Reynolds numbers (around 200). We recorded the position and orientation of each cylinder as it fell through still water, as well as the distribution of landing sites. We also performed planar particle image velocimetry to visualize wake dynamics. Results showed significant differences in the settling characteristics of uniform- vs compound-density cylinders, and revealed three distinct settling modes: rectilinear, oscillatory, and oblique. Each of the three modes displayed distinctly different wakes and vortex shedding patterns. All compound density cylinders, regardless of aspect ratio, were biased to land on the side of the tank, where the more dense end of the cylinder was initially oriented. Our results show that the interplay between buoyant torques and wake instability strongly impacts particle motion in the context of still-water settling, and is likely to play a role in more complex flows. This is true even for particles with an extremely small offset between the center of mass and the center of buoyancy, carrying strong implications for the dispersion of relevant particle classes such as microplastics.

DOI: [10.1103/PhysRevFluids.9.070501](https://doi.org/10.1103/PhysRevFluids.9.070501)

I. INTRODUCTION

Particles across a wide range of shapes and sizes play a key role in sediment transport, aerosol dispersion, marine aggregation, and many other processes [1–8]. Such particles are often irregular

*Contact author: mzb5025@psu.edu

in shape and composition, with a center of mass that is not at the volumetric center of the particle (i.e., its center of buoyancy). The settling dynamics of these particles—that is, nonspherical particles whose centers of mass (CoM) are not collocated with their centers of buoyancy (CoB)—are difficult to predict from first principles, particularly for particles settling at intermediate Reynolds numbers.

Particle Reynolds number is defined as $Re_p \equiv \frac{d_{eq}U}{\nu}$, where d_{eq} is an equivalent or representative particle diameter, U is a characteristic velocity (typically a terminal velocity in settling particles), and ν the kinematic viscosity of the carrier fluid. We chose the equivalent spherical diameter as the relevant length scale for consistency with other nonspherical particle literature (e.g., [9,10]) and because neither the cylinders' diameter nor the length consistently governed the observed particle settling behavior (see Results). Previous work on settling particles (both spherical and nonspherical) has primarily focused on Stokes flow ($Re_p \ll 1$) [11–15] and high Reynolds numbers ($Re_p \gg 1$) [16–20]. However, settling at intermediate Reynolds numbers ($1 < Re_p < 10^2$) is more difficult to characterize, though many particles in the natural and built environment fall into this regime (e.g., large sediment grains [21], marine aggregates [22–24], semipassive planktonic larvae [25–28], and microplastic pollutants [29,30]).

Microplastic particles, an increasingly common pollutant found throughout aquatic systems across the globe, exist in a wide variety of shapes including fibers, fragments, films, pellets, and more [31–34]. Their buoyancy can change due to degradation [35], aggregation with other particles [6,36,37], and biofouling [38–40]; these processes often occur asymmetrically due to consistently uneven exposure to air and light, leading to localized changes in mass density that displace the center of mass and complicate settling dynamics [41]. Because of this complexity, models of microplastic transport typically parametrize microplastics as spherical particles of uniform density [42], though shape or type (e.g. fibers vs fragments) could play a major role in transport [43].

Given the prevalence of nonuniform particles in various sedimentation processes, it is important to determine whether small changes in mass distribution can produce significant variations in settling. As a first step, we experimentally measure the settling velocity and time-varying orientation dynamics of low-aspect-ratio cylinders, comparing uniform (CoM collocated with CoB) vs nonuniform (CoM offset from CoB) cylinders with the same average mass density. Though we displace the CoM by less than 0.05% of the cylinder length, we find large differences between uniform vs nonuniform cylinders in both settling velocity and dispersion. This indicates that even extremely small changes to the location of the CoM—which may be the case for fouled or degraded microplastics—can lead to dramatic changes in settling velocity and overall settling behavior, which should be considered in efforts toward predictive modeling and analysis of existing observational data.

Below, we briefly review a selection of previous work on freely falling and rising bodies, with attention to cases relevant to low-aspect-ratio cylinders at intermediate Reynolds numbers and/or nonuniform mass distributions.

A. Uniform nonspherical particles

Freely falling or rising bodies, whose motion is driven by buoyancy, can exhibit complex behaviors even when traveling through a still fluid [44]. Trajectories may be chaotic or follow “zigzag” patterns, driven by vortical structures in the particle wakes [45,46]. While prolate and oblate ellipsoidal particles are frequently featured in numerical studies of nonspherical particles [47–51], cylinders (particularly disks) are commonly used for experimental studies due to greater ease of manufacturing [52–55]. Kanso *et al.* [53] experimentally showed that settling disks ($AR \equiv l/d < 1$, where l is cylinder length and d is cylinder diameter) experience four distinct settling regimes: steady, fluttering, chaotic, and tumbling, each of which lead to a unique distribution of landing sites and can be used to reliably predict what side of the disk is likely to land upright. Mandø and Rosendahl [19] determined that freely falling cylinders must fall with either a steady ($AR > 2$) or periodically varying ($AR < 2$) orientation (i.e., tumbling), with $Re_p > 100$ experiencing significant oscillatory motion regardless of aspect ratio due to wake instabilities. Komar [14] found an increased

drag coefficient for low-aspect-ratio cylinders compared to ellipsoids of equivalent aspect ratio, attributed to their relatively higher surface area. Marchildon *et al.* [56] studied the wakes of freely falling cylinders ($1.46 < \text{AR} < 35$) at $70 < \text{Re}_p < 2400$, and found that periodic oscillations were never present at $\text{Re}_p < 80$ and always present at $\text{Re}_p > 300$.

The onset of wake instabilities for finite bodies tends to occur at higher Reynolds numbers than infinite (two-dimensional) bodies [55]; the transition for freely falling bodies tends to occur at higher Reynolds numbers compared to fixed bodies [44]. For fixed bodies, vortex shedding begins around $\text{Re}_p = 212$ (spheres [57,58]), 116.5 (thin circular disks [57]), and 159.4 (thick disks [59]). For longer (but finite) cylinders ($\text{AR} > 1$) with free flat ends, vortex shedding is highly dependent on aspect ratio; the onset of vortex shedding varies from approximately $50 < \text{Re}_p < 300$ [57,60–62]. However, the freely falling case (where the body has six degrees of freedom to respond to fluid forcing) is more difficult to measure and simulate, particularly for nonspherical bodies [44]. Transition depends on density ratio, Archimedes or Galileo number, and particle geometry; for spheres, this may vary from $205 < \text{Re}_p < 310$ [63], and less is known for nonspherical shapes. Chung *et al.* [64] studied the wakes of tethered, low-aspect-ratio cylinders ($0.5 < \text{AR} < 2$), where a wire strung through the center of the cylinder allowed for one degree of freedom in a horizontal water channel. While not exactly analogous to settling, they showed three distinct modes as Re_p varied from 100 to 5000. Intermediate Re_p showed steady and periodic orientations, while high Re_p showed autorotation around the hinged axis. Recently, Toupoint *et al.* [65] examined the trajectories and wakes of freely falling cylinders near neutral buoyancy, with aspect ratios ranging from 2 to 20; their qualitative wake visualization revealed periodicity in the wake for Reynolds numbers as low as 50 (based on cylinder diameter; corresponding to $\text{Re}_p = 123$ based on equivalent-volume sphere diameter). The trajectories they observed somewhat matched those previously observed in the (somewhat better studied) spheres and disks: rectilinear, fluttering or zigzag, and an irregular transition between the two containing a richly complex suite of behaviors. In this work, we seek to extend the existing knowledge for cylinder sedimentation to cylinders with nonuniform mass distributions (while acknowledging there remains much to be discovered even for freely falling nonspherical bodies with uniform mass distributions).

B. Nonuniform nonspherical particles

Nonspherical particles with nonuniform mass distributions are understudied compared to uniform nonspherical particles, especially at intermediate Reynolds numbers. A strong motivating problem is that of nonuniform flocs or aggregates; however, the focus typically remains on the floc's porosity, and does not explore particles in which the CoM is nontrivially offset from the CoB [66–69]. Cui *et al.* [70] explicitly accounted for an offset CoM in stochastically formed flocs; they found that the additional gravitational torque caused rotation, which impacted orientation, which impacted drag, and therefore settling velocity.

Studies of cylinders in which the CoM is offset from the CoB have typically focused on higher Reynolds numbers and larger objects due to their relevance in industrial and military undersea applications. Yasserli *et al.* [71] examined the trajectory and landing sites of cylinders with variable CoM for which $9 \text{ cm} < l < 15 \text{ cm}$, $1 < \text{AR} < 2$, and $1 < v_s < 10 \text{ ms}^{-1}$; they found that the location of the CoM had a greater influence on landing site than initial inclination or AR. Abelev *et al.* [72] and Lan *et al.* [73] both found that higher displacement of the CoM increased terminal velocity in cylinders falling at high Re_p , in part by altering the stable terminal orientation of the cylinder. However, it is unclear how and whether these results will apply at intermediate Re_p , or across a wider range of aspect ratios. To fill this gap, we investigate settling cylinders with both uniform and nonuniform mass distributions with aspect ratios from 1 to 4, while specifically targeting an Re_p of approximately 200.

Our work deviates from the existing literature on falling cylinders in two key ways: first, we explore cylinders for which $1 \leq \text{AR} \leq 4$, so that our cylinders are too tall to be considered disks

TABLE I. Dimensions of cylinders (both UD and CD), equivalent-volume sphere diameter, predicted particle Reynolds numbers (using models from [10]), Galileo number (where $G \equiv \sqrt{(1 - \rho_p/\rho_f)gd_{\text{eq}}^3/\nu}$), and measured particle Reynolds numbers for UD cylinders, as well as percentage offset of the center of mass in the compound density case (distance of CoM to cylinder centroid, divided by cylinder length). N is the number of trials analyzed after discounting aberrant cases (from a total of 100), given for both UD and CD cylinders.

AR (-)	l (mm)	d (mm)	d_{eq} (mm)	Re_p (predicted)	G (-)	Re_p (actual, UD)	CoM offset (%, CD)	N (UD/CD)
1	8.0	8.0	9.2	207	198	244	0.05	97/100
2	14.0	7.0	10.1	228	229	275	0.05	100/96
4	24.0	6.0	10.9	215	257	255	0.05	100/93

and too thick to be considered fibers. Second, we consider cylinders of nonuniform mass density, finding that minute shifts in the center of mass of a cylinder can strongly affect its settling behavior.

II. METHODS

We tracked the position and orientation of cylinders as they fell through still water. All cylinders had the same average mass density, made with either a single uniform density (UD) or a compound density (CD), which we created using two joined half-cylinders with different mass densities. We fabricated cylinders with three aspect ratios ($\text{AR} = 1, 2, 4$) for a total of six cylinder classes (see Table I), and dropped 100 of each type to characterize their settling dynamics. Irregular trials (e.g., adhesion to dropping mechanism affecting settling behavior) were excluded from the analysis, resulting in 93–100 trials per cylinder class (see Table I). The cylinders were initially held at a horizontal orientation and released into a tall tank of still water. Two high-speed cameras imaged the cylinders far below the dropping point, which enabled three-dimensional tracking at terminal velocity. We also measured velocity fields around a subset of the falling cylinders in each settling regime using planar particle image velocimetry (PIV) to clarify the steady and unsteady wake dynamics leading to the observed settling behavior.

To facilitate imaging while tightly controlling particle density, we fabricated cylinders from agarose hydrogel. Agarose is a nontoxic hydrogel that is easily cast in different shapes across a wide range of mass densities that are close to that of water. Hydrogel also has nearly the same refractive index as water, and is therefore useful for laser-based flow visualization [74]. Hydrogel cylinders have also been recently used in several studies of nonspherical particle dynamics at intermediate Re_p [2,54,75–77].

Agarose powder (OmniPur Agarose, Calbiochem) was dissolved in distilled water heated to 80 °C. A prescribed volume of the heated solution was then injected into machined aluminum molds; UD cylinders were made by filling the entire mold with one (constant-density) hydrogel solution, while CD cylinders were made by half-filling the molds with a lower-density solution followed by a higher-density solution after 3 min. This procedure produced bonded CD cylinders that reliably did not separate during experiments. After both solutions were injected into the mold, the cylinders cooled at 20 °C for 10 min before being placed in a refrigerator (4.5 °C) for 3 min. Molds were coated with mineral oil to ease release of the completed cylinders. We used agarose concentrations of 0.008, 0.012, and 0.016 g/ml, which produced gels with specific gravities of 1.003, 1.005, and 1.007, respectively; hydrogel density was validated by drop-testing 1-cm spheres in still water and comparing their settling velocity to accepted theory (see Supplemental Material [78] including Refs. [10,15,63,79–88]). We targeted near-neutral buoyancy as this is the condition of many marine aggregates and microplastics, two major particle classes of interest. Furthermore, near-neutral buoyancy allowed us to use relatively large cylinders (for ease of fabrication) that settled slowly (for ease of imaging), while maintaining the target Re_p of approximately 200.

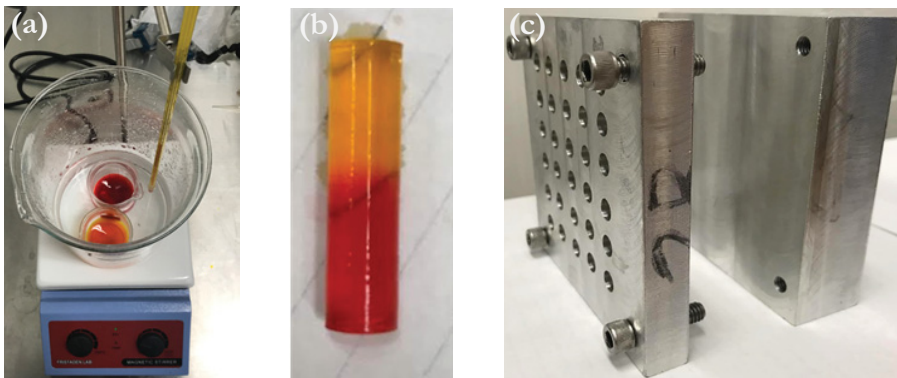


FIG. 1. Photographs of the cylinder fabrication process, showing (a) hot water bath and dissolving agarose solution, (b) a completed $AR = 4$ CD cylinder, and (c) the machined aluminum molds.

Cylinder properties are given in Table I. We chose cylinder dimensions such that we could achieve $AR = 1, 2,$ and 4 while maintaining volume (and therefore sphere-equivalent diameter) to within 10% variability, and predicted terminal Re_p of approximately 200. Re_p was predicted by using empirical drag models from [10] (see Supplemental Material [78]). An adjusted particle Reynolds number is defined as $Re_p^* = C_{\text{shape}} Re_p / f_{\text{shape}}$, where C_{shape} and f_{shape} are drag corrections based on the cylinder geometry, and Re_p is the quantity we are predicting. Re_p^* is then used to determine the Schiller-Naumann and Clift-Gauvin corrections, such that

$$C_D^* = [1 + 0.15(Re_p^{*0.687})] \left(\frac{24}{Re_p^*} \right) + \frac{0.42}{1 + \frac{42,500}{Re_p^{*1.16}}},$$

where $C_D^* = C_D / C_{\text{shape}}$. A steady-state force balance between gravity, buoyancy, and drag relates the resulting C_D to the expected terminal settling velocity, v (which itself determines Re_p). The particle geometry, which affects the predicted C_D , can then be iteratively adjusted until the desired Re_p is reached (as described in the Supplemental Material [78]). However, this does not ensure that different aspect-ratio cylinders have the same equivalent diameter d_{eq} . Thus, we select the cylinder geometry so that there is no more than 10% variation in either d_{eq} or Re_p (Table I).

The targeted Reynolds number represents the approximate onset of oscillatory wake development as outlined in the previous section. The average specific gravity of both UD and CD cylinders was 1.005; the CD cylinder halves had specific gravities of 1.003 and 1.007. The Galileo number (representing the ratio of buoyancy to viscosity) ranges from 198 to 257 based on the overall specific gravity and the equivalent-volume sphere diameter. Cylinders were lightly dyed to facilitate visualization during trajectory measurement; the presence of the dye did not affect the overall density. Undyed cylinders were used during PIV measurements to avoid occlusion of the laser sheet. Figure 1 shows photographs of the fabrication process.

A. Trajectory measurement

Particles were released from a pair of modified forceps at the top of a hexagonal water tank (61 cm in height with 53 cm between parallel sides), as shown in Fig. 2. Two high-speed cameras (AX200, Photron), filming at 500 fps, captured cylinder orientation and position through overlapping 15×15 cm fields of view centered 37.5 cm below the dropping mechanism; their optical axes were separated by 120° in order to capture three-dimensional cylinder motion. In these fields of view, vertical velocity was consistent throughout the field of view for UD cylinders (see Fig. 10); terminal velocity/behavior may therefore be assumed. The forceps were positioned just below the water surface (56 cm above the bottom of the tank) and fitted with plates to hold

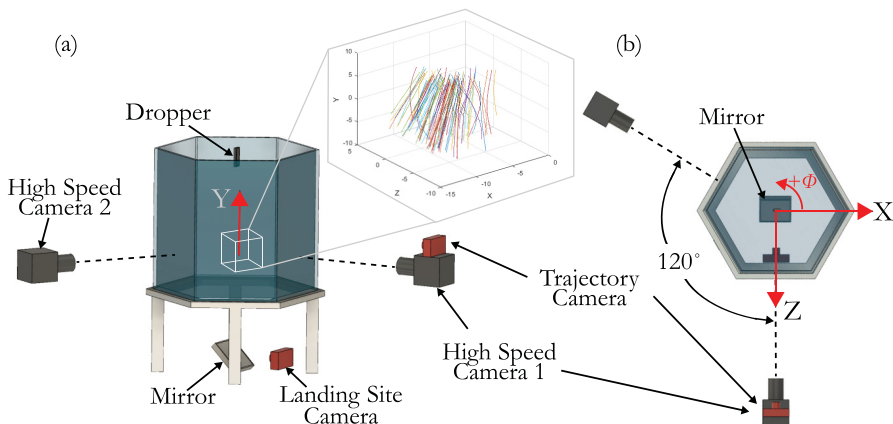


FIG. 2. Experimental setup, showing high-speed cameras, low-speed cameras, dropping mechanism, and mirror used to visualize landing sites from side view (a) and top view (b). Inset shows an example of three-dimensional trajectories of falling cylinders (reconstructed from recordings from two high-speed cameras) as they fall through the white-outlined volume. The global x and z axes are shown in the top view (b); the y axis is vertical and Φ denotes rotation about the y axis.

each cylinder horizontal upon release; the axis of symmetry was nearly perpendicular to the optical axis of high-speed camera 1 (with the denser end on the left for CD cylinders). Two LED light panels provided illumination for the high-speed cameras. A low-speed camera (RX100M4, Sony) was positioned directly on top of high-speed camera 1 to capture an enlarged view of the tank to qualitatively visualize the entire cylinder trajectory. A second low-speed camera (RX100M4, Sony) imaged the bottom of the tank via a mirror angled at 45° ; this camera recorded the landing site for each cylinder.

We used the simultaneous recordings from both high-speed cameras to calculate the cylinder position and orientation as a function of time. Images were contrast enhanced and binarized to distinguish the cylinder from the background, with additional preprocessing steps to remove noise. From these images, we tracked the cylinder's centroid location and major axis orientation in each camera plane. To enable three-dimensional position and orientation tracking, we calibrated the two cameras via an image of a three-level calibration plate with 50 mm between levels and 20 mm between calibration points [87]. Forty-eight points, visible in both camera views, mapped the image plane of each camera to global space using direct linear transformation [88]. Because the cylinders did not significantly rotate about the global y axis (i.e., the variance in the azimuthal angle Φ was low), we used the horizontal inclination angle from the projected view of high-speed camera 1 as the basis for the analysis that follows. Further details are given in the Supplemental Material [78].

B. Particle image velocimetry

Representative flow fields around each cylinder class were also quantified in separate experiments using PIV. These measurements allowed us to identify the steady and unsteady vortex structures in the wake of the falling cylinders that contributed to the observed settling behavior. For these experiments, the water was seeded with $55\text{-}\mu\text{m}$ polyamide spheres, which served as flow tracers. High-speed camera 1 was used to capture planar PIV measurements of the cylinders and the surrounding flow at an effective frame rate of 50 fps ($\Delta t = dt = 0.02$ s). The flow field was illuminated using a planar laser light sheet (approximately 0.2 mm thick), created by a continuous-wave green laser (Opus 532, Laser Quantum) introduced through the bottom of the tank and oriented perpendicular to the optical axis of high-speed camera 1.

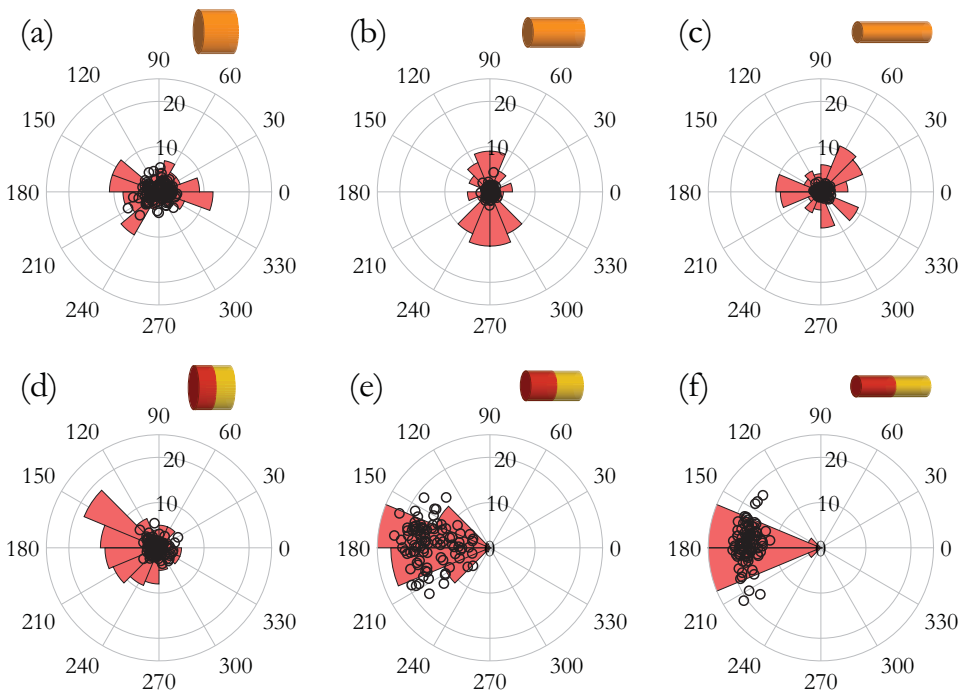


FIG. 3. (a)–(e) Landing sites of six cylinder classes (black circles) overlaid on an angular histogram of azimuthal position (bin size 20°). The outer edge of the histogram shows angles marked in degrees; labeling of rings represents the radial distance from center in cm (for landing sites) and the number of cylinders in each angular bin (for histogram). The histogram extends beyond the bounds of the plot in panels (e) and (f).

All PIV analysis was performed in the open source program PIVLAB [89], a MATLAB toolbox (Mathworks, Inc). Images were preprocessed within PIVLAB using an enhanced local contrast filter with a 20×20 pixel window size, followed by a high-pass filter with a 15×15 pixel kernel. Multipass processing (with interrogation areas of 64×64 , 32×32 , and 24×24 pixels, each with a 50% overlap) provided a final measurement resolution of 1.9×1.9 mm. Postprocessing included the removal of any velocity vectors greater than 15 standard deviations above the average velocity vector in each image. Out-of-plane vorticity in the flow was calculated from velocity vectors smoothed with a penalized least-squares method [90]; vorticity ($\omega_z = \frac{\partial v}{\partial x} - \frac{\partial u}{\partial y}$ where u is the x -velocity component and v is the y -velocity component) was then used to qualitatively evaluate wake structures around each cylinder.

III. RESULTS

Settling behavior was distinctly different between the UD and CD cylinders of identical aspect ratio, though the center of mass was shifted by only 0.05% of the overall cylinder length. We observed several distinct modes that led to shifts in the landing site distribution, varying with composition and aspect ratio.

A. Landing sites

Figure 3 shows the landing sites for the UD and CD cylinders for each aspect ratio. Each black circle shows the landing site of an individual cylinder; an overlaid angular histogram plot shows the distribution of the landing sites' azimuthal angle for each cylinder type (measured relative to the

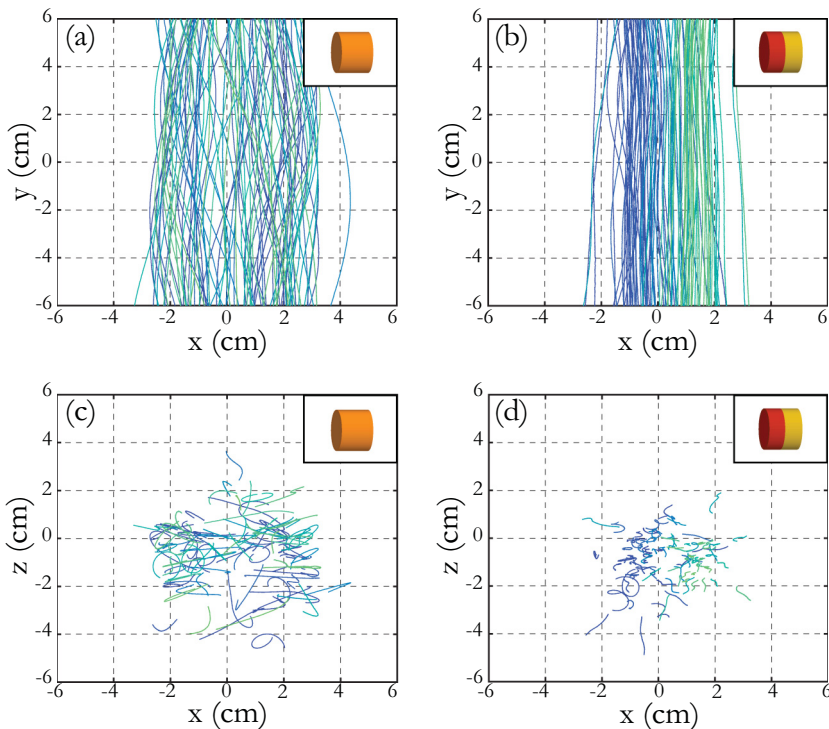


FIG. 4. Falling trajectories for cylinders with $AR = 1$. (a), (b) show trajectories in the x - y plane of UD and CD cylinders, respectively; (c), (d) show the x - z plane. Color variation indicates different trials ($N = 100$) to assist in visualization.

positive x axis). In general, UD cylinders were clustered tightly around the tank center ($r = 0$) with no clear azimuthal distribution; in contrast, CD cylinders moved to the left, where the denser end of the cylinder was initially oriented, and landed further away from the tank axis. This leftward drift increased with aspect ratio, with higher variability seen for $AR = 2$.

B. Cylinder trajectories and orientations

We tracked centroid locations (x_c, y_c, z_c) and orientation of the principal axis with respect to the horizontal (θ) for all six cylinder classes. Figure 4 shows the centroid locations for $AR = 1$ cylinders as they descended through the field of view. UD cylinders showed slightly higher lateral variation, with some long-period oscillation in the x position. This can be attributed in part to falling orientation (Fig. 5). The UD cylinders did not display a consistent orientation; some fell broadside ($\theta \sim 0^\circ$) without oscillation, others oscillated about a broadside position ($-50^\circ < \theta < 50^\circ$), and still others oscillated about a near-vertical position ($45^\circ < \theta < 150^\circ$). By contrast, CD cylinders stabilized in a vertical orientation ($\theta \sim 90^\circ$) with the denser end pointing down, with some smaller-amplitude oscillation around this position. This indicates that the CD cylinders rotated 90° after release from an initially horizontal position; inertia may lead to an overshoot of the stable vertical position, leading to the observed oscillations in Fig. 5(b).

Uniform density cylinders typically settle with a preferred orientation that maximizes their projected area in the direction of settling up to $Re_p = 100$ [19]. It is therefore unsurprising that the UD cylinders at $AR = 1$ did not display a single preferred fall orientation, given that the vertical orientation's projected area is only 24% less than the horizontal orientation's (by contrast, at $AR = 2$, this difference is 87%). This lack of a definitive preferred orientation for UD cylinders

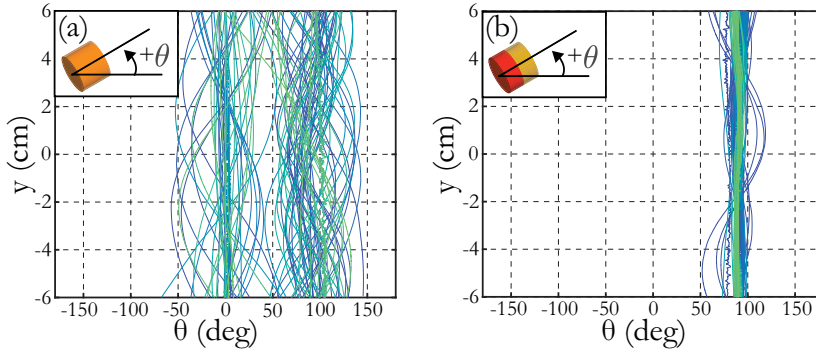


FIG. 5. Major axis orientation for all trials of both $AR = 1$ cylinder classes, showing (a) UD cylinders and (b) CD cylinders.

at $AR = 1$ led to a higher variation in lateral position compared to $AR = 2$ and 4 , which can also be observed in Fig. 3(a) vs Figs. 3(b) and 3(c).

Figure 6 shows trajectories for cylinders with $AR = 2$. As in $AR = 1$, the UD and CD cylinders displayed different settling behaviors. The UD cylinders fell straight down with little lateral variation. However, two distinct modes can be seen in the CD cylinders: some fell steadily downward

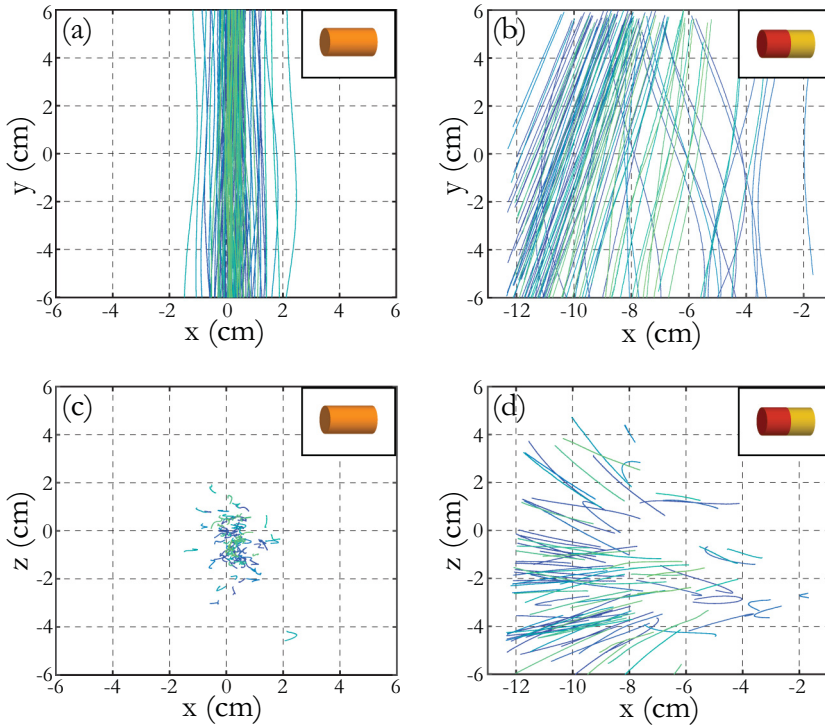


FIG. 6. Falling trajectories for cylinders with $AR = 2$. (a) and (b) show trajectories in the x - y plane of UD and CD cylinders, respectively; (c) and (d) show the x - z plane. Color variation indicates different trials ($N = 100$) to assist in visualization. Note that the x axis shifts to the left for panels (b) and (d) to accommodate leftward drift of CD cylinders prior to entering the field of view.

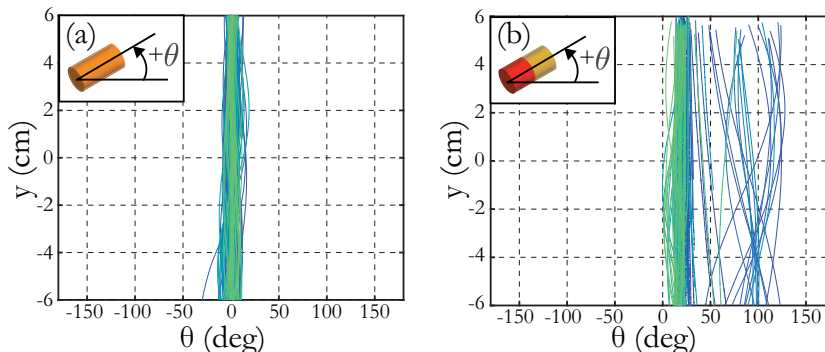


FIG. 7. Major axis orientation for all trials of both $AR = 2$ cylinder classes, showing (a) UD cylinders and (b) CD cylinders.

and to the left, while others showed more vertical trajectories with a long-period lateral oscillation as they fell. This is also visible in the cylinder orientations (Fig. 7): UD cylinders maintained a steady horizontal orientation ($\theta \sim 0^\circ$) while CD cylinders again showed two modes. Most of the CD cylinders held a constant orientation angle around $\theta = 19^\circ$ throughout the entire field of view, drifting to the left throughout the observed period. However, some CD cylinders fell vertically ($\theta \sim 90^\circ$) and oscillated about this orientation, similarly to the CD cylinders at $AR = 1$. A small number of cylinders appeared to be transitioning between the two modes, with initially left-slanted trajectories curving to the right as they exit the measurement domain.

Figure 8 shows the trajectories for cylinders with $AR = 4$. As in the previous case, the UD cylinders settled vertically with little lateral variation. The CD cylinders all fell with slanted trajectories, and did not display multiple modes (as in the CD cylinders at $AR = 2$). Orientations (Fig. 9) were also consistent, with all UD cylinders falling horizontally ($\theta \sim 0^\circ$) and all CD cylinders falling at a constant orientation angle of approximately $\theta = 9.5^\circ$. This angle is shallower than the average stable angle of the subgroup of CD cylinders at $AR = 2$, which also had slanted trajectories.

C. Cylinder velocity

In addition to time-varying position and orientation, we calculated the average vertical velocity \bar{v} for each cylinder class (Fig. 10). We separated CD cylinders at $AR = 2$ into two subgroups, as they displayed two distinct settling modes and therefore two very different settling velocities. A total of 71/100 cylinders settled with a maximum angle from the horizontal of $\theta_{\max} < 35^\circ$ and were placed in the first subgroup (slanted trajectories); 18/100 cylinders had $\theta_{\max} > 75^\circ$ and were placed in the second subgroup (oscillating trajectories). The remaining 11/100 cylinders had $35^\circ < \theta_{\max} < 75^\circ$, which we defined to be transitional; they are not included in Fig. 10. In general, CD cylinders that fell in a vertical orientation with oscillating trajectories fell the fastest, with $AR = 2$ falling faster than $AR = 1$. For the remainder of the classes, the cylinders with the smallest projected area in the vertical direction fell fastest and the cylinders with the largest projected area fell slowest. We note that the cylinders that fell in a stable, slanted orientation (the first subgroup of $AR = 2$ CD cylinders and $AR = 4$ CD cylinders) fell more slowly than their UD counterparts, but had a nontrivial lateral velocity.

D. Particle image velocimetry

To clarify the possible influence of wake structure on settling behavior, we performed planar PIV. Because the hydrogel cylinders were refractive index matched to water, and we used an undyed cylinder for the PIV measurements, the laser sheet passed through them unoccluded and enabled

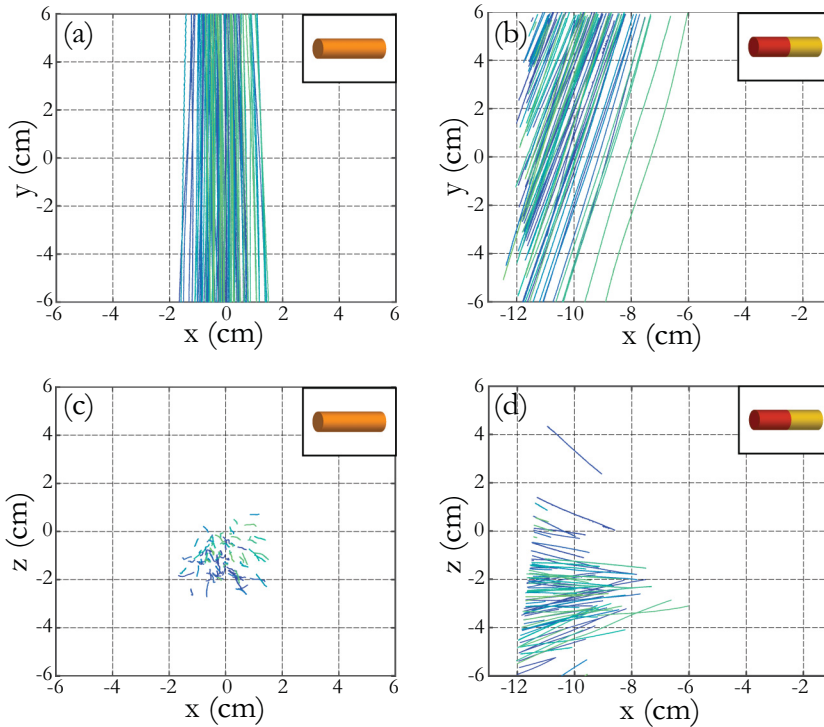


FIG. 8. Falling trajectories for cylinders with $AR = 4$. (a) and (b) show trajectories in the x - y plane of UD and CD cylinders, respectively; (c) and (d) show the x - z plane. Color variation indicates different trials ($N = 100$) to assist in visualization. Note that the x axis shifts to the left for panels (b) and (d) to accommodate leftward drift of CD cylinders prior to entering the field of view.

visualization around the entire falling body. Figure 11 shows contours of out-of-plane vorticity ω_z for three distinct settling behaviors. The first behavior, in which cylinders fell straight down with no change in orientation angle, is typified by UD cylinders at $AR = 4$ [Fig. 11(a)]. Symmetric vortex rings behind the cylinder, identified by the regions of opposite-signed vorticity located behind each end of the cylinder, appear to have been shed at regular intervals as the cylinder settled

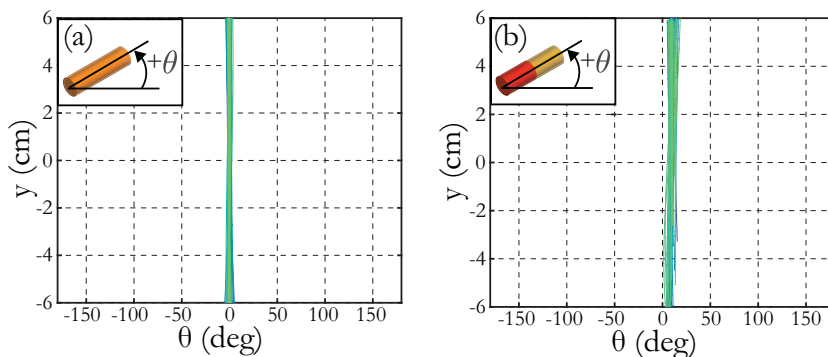


FIG. 9. Major axis orientation for all trials of both $AR = 4$ cylinder classes, showing (a) UD cylinders and (b) CD cylinders.

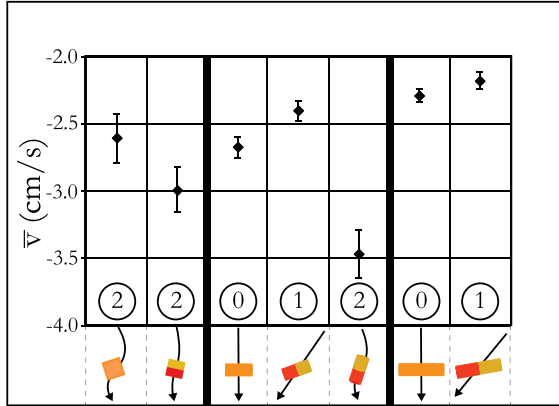


FIG. 10. Average vertical velocities for the six cylinder classes (AR = 1, 2, and 4 for both compound density and uniform density), with CD cylinders at AR = 2 separated into two subgroups (determined by maximum achieved orientation angle during observation). For this case, cylinders are broken into mode 1 (71%) and mode 2 (18%); transitional cases (11%) are not shown. Numbered circles indicate falling modes as discussed in Sec. IV. Error bars represent one standard deviation.

through the water. These vortex rings detached periodically and decreased in strength over time after being shed. The UD cylinders at AR = 2 (not shown), which also fell with a similar stable horizontal orientation, had similar wake structures, which is typical for this type of stable horizontal settling [65].

The second behavior, in which cylinders fall at a fixed angle with a slanted trajectory (but with little to no oscillation), is typified by CD cylinders at AR = 4 [Fig. 11(b)]. On the top leading edge of the cylinder, a region of positive vorticity (likely caused by an attached vortex) remained

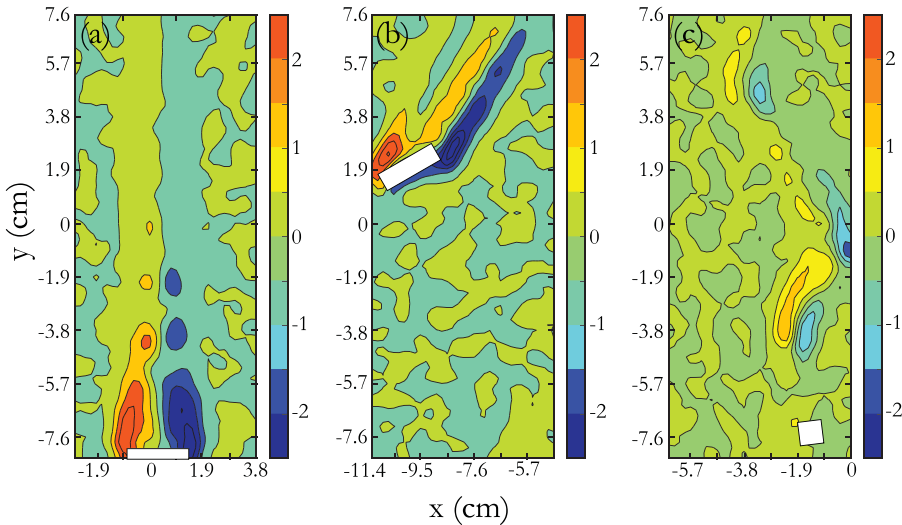


FIG. 11. Contour plots of out-of-plane vorticity ω_z (s^{-1} , scale in color bar) for cylinder classes falling with different settling behaviors, including (a) straight and horizontal, exemplified by UD cylinders at AR = 4; (b) straight and angled, exemplified by CD cylinders at AR = 4; and (c) oscillating about a vertical orientation, here shown with a CD cylinder at AR = 1.

present and attached as the cylinder passed through the measurement domain. A second region of interest is located behind the trailing edge of the cylinder, where we observed two patches of opposite-signed vorticity. However, the positive vorticity in this pair is weaker (1.5 s^{-1}) than the negative vorticity (2.5 s^{-1}). Some evidence of vortex shedding can be seen in the trailing-edge region, but the leading-edge vortex remains attached, which is indicative of lift generation [91]. As shown in Fig. 8(b), these cylinders fall at a trajectory angled approximately 55° from the horizontal, resulting in an angle of attack of around 45° —enough to produce nontrivial lift forces that may counter the hydrostatic restoring torque from the offset center of mass.

The third behavior, in which cylinders fall in a primarily vertical orientation with some periodicity in their trajectory and orientation, is shown by CD cylinders at $\text{AR} = 1$ [Fig. 11(c)]. This cylinder shed several pairs of vortices as it settled. The vortex pairs were shed at the three locations where the cylinder changed directions over the course of its periodic trajectory through the field of view [specifically, these vortex structures can be seen at the locations $(x, y) = (-3, 5)$, $(-1, 0)$, and $(-1.9, 3.8)$ cm]. From this, we conclude that a pair of vortices are shed every time a cylinder with an oscillatory trajectory cylinder changes direction in free fall. We note that the vorticity shown in Fig. 11(c) is relatively weak when compared to Figs. 11(a) and 11(b); this is due to the smaller cylinder dimensions, which leads to shear stresses and vorticity that are smaller in magnitude. Videos of the falling cylinders, together with time-varying velocity and vorticity fields, are available in the Supplemental Material [78].

IV. DISCUSSION

We have identified three settling modes in falling cylinders at intermediate Reynolds numbers: (0) vertical trajectory, horizontal orientation (rectilinear); (1) slanted trajectory, angled orientation (oblique); and (2) vertical trajectory, oscillating orientation (oscillating). UD cylinders at $\text{AR} = 2$ and $\text{AR} = 4$ settle in mode 0. The settling behavior of these cylinders is similar to other elongated particles of finite size, and their settling velocity can be reasonably approximated using existing models (e.g., [76]). In contrast, the settling behavior of the other aspect ratios and density variations is more complex. Compound density cylinders at $\text{AR} = 4$ settle in mode 1, whereas CD cylinders at $\text{AR} = 1$ settle in mode 2. Some UD cylinders at $\text{AR} = 1$ settle in a variation of mode 0 (in which the cylinder orientation oscillates around a horizontal position and the trajectory displays some periodicity), while other cylinders in the same class settle in mode 2; as previously discussed, the lack of a dominant mode in this class is likely due to the small difference in projected area between a vertically and horizontally oriented cylinder at $\text{AR} = 1$. Unlike the CD cylinders at $\text{AR} = 2$, the two modes cannot be cleanly separated by maximum orientation angle; there appears to be a relatively smooth transition between the two modes. The vertically oriented cylinders with $\text{AR} = 1$ appear similar, in both trajectory and wake structure, to previously studied flat cylinders/thick disks [92,93].

CD cylinders at $\text{AR} = 2$ settle in both mode 1 and mode 2, with a small transition group. While some differences may be attributed to minor inconsistency in cylinder fabrication, the differences are dramatic (including a nearly 50% increase in overall settling velocity). This indicates the presence of some kind of transition threshold, which may be driven by oscillatory wake dynamics that are likely to be dependent on Re_p . To further explore potential mechanisms leading to transition, we qualitatively observed the settling of additional CD cylinders at $\text{AR} = 2$ —this time directly varying Re_p by manipulating the water temperature (and therefore density and viscosity). When water was chilled to 1.5°C (increasing kinematic viscosity by 70% relative to 20°C), 93% of cylinders ($N = 28$) fell in mode 1 with the remainder showing transitional behavior. When the water was heated to 36.5°C (decreasing the kinematic viscosity by 30% relative to 20°C), 100% of cylinders ($N = 27$) fell in mode 2.

Further evidence of a critical Reynolds number transition can be seen in Fig. 12, which shows a nonoverlapping range of Reynolds numbers between mode 1 and mode 2 for this cylinder class. We

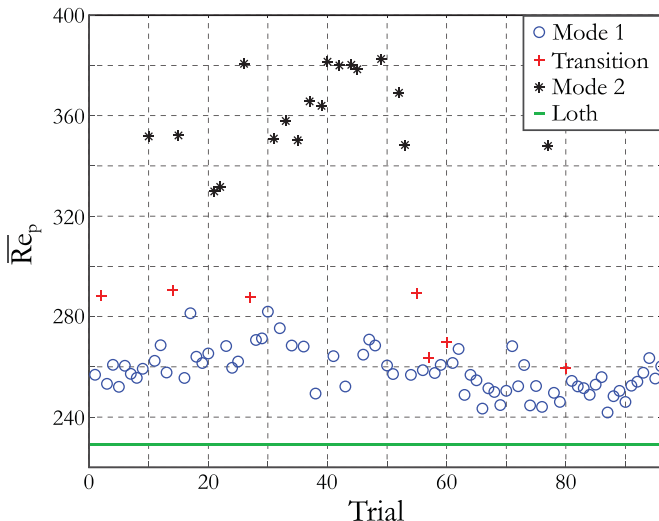


FIG. 12. Particle Reynolds number (based on average speed and volume-equivalent sphere diameter) for CD cylinders at $AR = 2$ falling in 20°C water. Cylinders falling in mode 1 (\circ) had Re_p below 285; cylinders falling in mode 2 ($*$) had Re_p above 330; transitional cylinders ($+$) fell in-between. All cylinders ($N = 96$) fell at higher Reynolds numbers than that predicted by empirical models outlined by Loth [10] ($-$).

note that this is descriptive, not prescriptive; further information is needed to definitively outline an underlying mechanism. However, we hypothesize the following: an initially horizontal CD cylinder tilts initially toward its denser end, decreasing flow-normal area, drag, and increasing overall settling velocity—and therefore increasing Reynolds number relative to the horizontal case (this can also be seen in Fig. 12, where all cylinders fall at higher Re_p than predicted by a model that assumes uniform mass distribution). At this point, one of two outcomes is possible. In the first case, an attached vortex [as shown in Fig. 11(b)] provides lift, countering the restoring torque caused by the CoM offset and causing the cylinder to fall in a stable orientation, drifting laterally as it settles (mode 1). In the second case, there is vortex shedding in the cylinder wake [as seen in Fig. 11(c)], and the cylinder rotates further into a hydrostatically stable vertical orientation, with inertia causing a slight overshoot and subsequent oscillation about that vertical orientation (mode 2). The bifurcation may potentially be explained with two governing timescales: the timescale of the attached vortex development, τ_v , vs the timescale of the rotation induced by buoyant torques, τ_b . If $\tau_v \ll \tau_b$, slow rotation would allow for the development of the attached vortex (which then would counteract the buoyant torque and stabilize the cylinder at a fixed orientation angle, as in mode 1). If $\tau_v \gg \tau_b$, the attached vortex would not have time to develop and the cylinder would descend in mode 2. Further work, including more detailed flow visualization, is needed to quantify both timescales and to explore the case in which $\tau_v \sim \tau_b$; we hypothesize that both τ_v and τ_b are likely to depend strongly on Re_p .

The presence or absence of this bifurcation point between modes 1 and 2 (and the approximate Re_p at which it occurs) is also likely to depend strongly on both the CoM offset and the particle's aspect ratio; for example, in our experiments, we did not observe bimodal behavior in CD cylinders at $AR = 4$, which all fell in mode 1. Previous work has shown that even slight differences to a cylinder's moment of inertia can trigger dramatic shifts in behavior and wake instability, in part because the rotational degree of freedom about the axis of symmetry can cause the shear layer to remain attached for longer, thereby lowering the shedding frequency [94]. However, our flow visualization plane was normal to the axis of symmetry, precluding observation of these effects. While the planar visualization discussed here is useful for an initial categorical description of

important vortex-dominated phenomena (such as the transition between mode 1 and mode 2 as discussed above), a full treatment of the problem will necessitate more well-resolved measurements of the cylinder wakes. Future work with three-dimensional flow visualization and measurement could shed light on the role of the shifted center of mass, particularly near transitional Reynolds numbers.

We note that the initial cylinder orientation, which was not varied here, likely also plays a role in the settling mode of these near-transition cylinders. We expect that an initially vertical orientation, with the more dense side of the cylinder below the less dense end, would produce mode 2 settling behavior as the initial generation of the attached vortex characteristic of mode 1 would be avoided (see previous discussion). However, the universality of this hypothesis to cylinders with higher aspect ratios requires further investigation. As previously discussed, there is a tendency for bodies to settle in a drag-maximizing orientation: uniform-density cylinders with high aspect ratios will terminally settle in a horizontal orientation (mode 0), no matter their initial orientation [10,14]. However, a displaced center of mass produces a buoyant torque; the greater the offset, the greater the buoyant torque. There is then a balance between drag-maximizing torque (driven by aspect ratio) and buoyant torque (driven by CoM offset), both of which are dependent on Re_p . We hypothesize that initial orientation plays an important role when these two torques are of the same order, which is likely the case for the $AR = 2$ CD cylinders discussed in this study.

V. CONCLUSIONS

We measured the landing sites, position, and orientation of falling cylinders of both uniform and nonuniform density across several aspect ratios ($1 \leq AR \leq 4$). Nonuniform (compound) cylinders generally had much higher net lateral motion, even though the center of mass was shifted by less than 0.05% of the cylinder length. This carries strong implications for particle dispersion in natural and industrial environments, particularly in the context of microplastics. Nonuniformity is common, and often highly localized; because of the inherent directionality of light and air availability, biofouling and degradation processes may add or subtract small amounts of mass in some regions more strongly than others. Even these small changes in mass distribution may be enough to dramatically increase overall dispersion of particles.

In the cylinders tested here, we observed three distinct settling modes: horizontal orientation/vertical trajectory (mode 0), tilted orientation/angled trajectory (mode 1), and vertical-oscillating orientation/laterally periodic trajectory (mode 2). Transitions between these modes, even within the same cylinder class, led to large changes in overall settling velocity. This again is strongly relevant to microplastic pollution: small localized additions of mass may increase settling velocity far above what would be predicted by a small increase in the overall particle density. The combination of nonsphericity, even at low aspect ratios, together with nonuniformity of mass distribution, can significantly alter settling velocities (see Fig. 10).

Further study is needed to clarify the role of mass distribution in settling nonuniform, nonspherical particles at intermediate Reynolds numbers. Three-dimensional flow visualization across a wider range of aspect ratios, mass distributions, and initial conditions should examine wake structure and its role in determining the orientation and trajectory of such particles as they fall. Visualization of trajectories over a larger region and longer period of time may also clarify how and why such miniscule changes in mass distribution can lead to dramatic changes to settling velocity and particle dispersion.

ACKNOWLEDGMENT

The authors acknowledge and appreciate assistance from Adrian Herrera-Amaya. B.R.A. conducted experiments, performed analysis, and wrote the first draft of the manuscript. M.J.R. and M.L.B. conceptualized the work, supervised experiments, and edited the manuscript. M.L.B. oversaw the overall analysis and editing process.

-
- [1] E. Deal, J. G. Venditti, S. J. Benavides, R. Bradley, Q. Zhang, K. Kamrin, and J. T. Perron, Grain shape effects in bed load sediment transport, *Nature (London)* **613**, 298 (2023).
- [2] M. Byron, J. Einarsson, K. Gustavsson, G. Voth, B. Mehlig, and E. Variano, Shape-dependence of particle rotation in isotropic turbulence, *Phys. Fluids* **27**, 035101 (2015).
- [3] A. L. Alldredge and C. C. Gotschalk, Direct observations of the mass flocculation of diatom blooms: Characteristics, settling velocities and formation of diatom aggregates, *Deep Sea Res., Part A* **36**, 159 (1989).
- [4] S. K. Beal, Deposition of particles in turbulent flow on channel or pipe walls channel or pipe walls, *Nucl. Sci. Eng.* **40**, 1 (2017).
- [5] T. Takahashi, Debris flow, *Ann. Rev. Fluid Mech.* **13**, 57 (1981).
- [6] M. Long, B. Moriceau, M. Gallinari, C. Lambert, A. Huvet, J. Raffray, and P. Soudant, Interactions between microplastics and phytoplankton aggregates: Impact on their respective fates, *Mar. Chem.* **175**, 39 (2015).
- [7] Z. Wang, S. Ren, and N. Huang, Saltation of non-spherical sand particles, *PLoS One* **9**, e105208 (2014).
- [8] A. R. Nayak, H. Jiang, M. L. Byron, J. M. Sullivan, M. N. McFarland, and D. W. Murphy, Editorial: Small scale spatial and temporal patterns in particles, plankton, and other organisms, *Front. Mar. Sci.* **8**, 669530 (2021).
- [9] G. A. Voth and A. Soldati, Anisotropic particles in turbulence, *Annu. Rev. Fluid Mech.* **49**, 249 (2017).
- [10] E. Loth, Drag of non-spherical solid particles of regular and irregular shape, *Powder Technol.* **182**, 342 (2008).
- [11] Thomas J. Hanratty and A. Bandukwala, Fluidization and sedimentation of spherical particles, *Am. Inst. Chem. Eng.* **3**, 293 (1957).
- [12] K. O. L. F. Jayaweera and B. J. Mason, The behaviour of freely falling cylinders and cones in a viscous fluid, *J. Fluid Mech.* **22**, 709 (1965).
- [13] P. D. Reimers and C. E. Komar, Grain shape effects on settling rates, *J. Geol.* **86**, 193 (1978).
- [14] P. D. Komar, Settling velocities of circular cylinders at low Reynolds numbers, *J. Geol.* **88**, 327 (2018).
- [15] D. Leith, Drag on nonspherical objects, *Aerosol Sci. Technol.* **6**, 153 (1987).
- [16] D. G. Karamanev, Equations for calculation of the terminal velocity and drag coefficient of solid spheres and gas bubbles, *Chem. Eng. Commun.* **147**, 75 (1996).
- [17] N. Mordant and J. F. Pinton, Velocity measurement of a settling sphere, *Eur. Phys. J. B*, **18**, 343 (2000).
- [18] G. Bagheri and C. Bonadonna, On the drag of freely falling non-spherical particles, *Powder Technol.* **301**, 526 (2016).
- [19] M. Mandø and L. Rosendahl, On the motion of non-spherical particles at high Reynolds number, *Powder Technol.* **202**, 1 (2010).
- [20] W. C. Krumbein, Settling-velocity and flume-behavior of non-spherical particles, *Trans., Am. Geophys. Union* **23**, 621 (1942).
- [21] G. H. Good, P. J. Ireland, G. P. Bewley, E. Bodenschatz, L. R. Collins, and Z. Warhaft, Settling regimes of inertial particles in isotropic turbulence, *J. Fluid Mech.* **759**, R3 (2014).
- [22] A. B. Bochdansky, M. A. Clouse, and G. J. Herndl, Dragon kings of the deep sea: Marine particles deviate markedly from the common number-size spectrum, *Sci. Rep.* **6**, 22633 (2016).
- [23] M. M. Mrokowska, Influence of pycnocline on settling behaviour of non-spherical particle and wake evolution, *Sci. Rep.* **10**, 20595 (2020).
- [24] J. C. Prairie, K. Ziervogel, R. Camassa, R. M. Mclaughlin, B. L. White, C. Dewald, and C. Arnosti, Delayed settling of marine snow: Effects of density gradient and particle properties and implications for carbon cycling, *Mar. Chem.* **175**, 28, (2015).
- [25] P. H. Lenz, D. Takagi, and D. K. Hartline, Choreographed swimming of copepod nauplii, *J. R. Soc., Interface* **12**, 20150776 (2015).
- [26] F.-S. Chia, J. Buckland-Nicks, and C. M. Young, Locomotion of marine invertebrate larvae: A review, *Can. J. Zool.* **62**, 1205 (1984).
- [27] H. L. Fuchs, E. J. Hunter, E. L. Schmitt, and R. A. Guazzo, Active downward propulsion by oyster larvae in turbulence, *J. Exp. Biol.* **216**, 1458 (2013).

- [28] M. H. DiBenedetto, K. R. Helfrich, A. Pires, E. J. Anderson, and L. S. Mullineaux, Responding to the signal and the noise: Behavior of planktonic gastropod larvae in turbulence, *J. Exp. Biol.* **225**, jeb243209 (2022).
- [29] M. H. Dibenedetto, L. K. Clark, N. Pujara, M. H. Dibenedetto, L. K. Clark, and N. Pujara, Enhanced settling and dispersion of inertial particles in surface waves, *J. Fluid Mech* **936**, 38 (2022).
- [30] K. Waldschläger and H. Schüttrumpf, Effects of particle properties on the settling and rise velocities of microplastics in freshwater under laboratory conditions, *Environ. Sci. Technol.* **53**, 1958 (2019).
- [31] K. Waldschläger and H. Schüttrumpf, Infiltration behavior of microplastic particles with different densities, sizes, and shapes—From glass spheres to natural sediments, *Environ. Sci. Technol.* **54**, 9366 (2020).
- [32] S. Rezanian, J. Park, M. F. Md Din, S. Mat Taib, A. Talaiekhosani, K. Kumar Yadav, and H. Kamyab, Microplastics pollution in different aquatic environments and biota: A review of recent studies, *Mar. Pollut. Bull.* **133**, 191 (2018).
- [33] R. Z. Miller, A. J. R. Watts, B. O. Winslow, T. S. Galloway, and A. P. W. Barrows, Mountains to the sea: River study of plastic and non-plastic microfiber pollution in the northeast USA, *Mar. Pollut. Bull.* **124**, 245 (2017).
- [34] R. Dris, J. Gasperi, M. Saad, C. Mirande, and B. Tassin, Synthetic fibers in atmospheric fallout: A source of microplastics in the environment? *Marine Pollution Bull.* **104**, 290 (2016).
- [35] A. L. Andrady, The plastic in microplastics: A review, *Mar. Pollut. Bull.* **119**, 12 (2017).
- [36] J. Michels, A. Stippkugel, M. Lenz, K. Wirtz, and A. Engel, Rapid aggregation of biofilm-covered microplastics with marine biogenic particles, *Proc. R. Soc. B.* **285**, 20181203 (2018).
- [37] A. Porter, B. P. Lyons, T. S. Galloway, and C. Lewis, Role of marine snows in microplastic fate and bioavailability, *Environ. Sci. Technol.* **52**, 7111 (2018).
- [38] S. Oberbeckmann, M. G. J. Löder, and M. Labrenz, Marine microplastic-associated biofilms—A review, *Environ. Chem.* **12**, 551 (2015).
- [39] C. Tu, Q. Zhou, C. Zhang, Y. Liu, and Y. Luo, Biofilms of microplastics, in *Handbook of Environmental Chemistry* (Springer Science and Business Media Deutschland GmbH, Berlin, 2020), Vol. 95, pp. 299–317.
- [40] A. L. Andrady, Microplastics in the marine environment, *Mar. Pollut. Bull.* **62**, 1596 (2011).
- [41] I. Jalón-Rojas, A. Romero-Ramírez, K. Fauquembergue, L. Rossignol, J. Cachot, D. Sous, and B. Morin, Effects of biofilms and particle physical properties on the rising and settling velocities of microplastic fibers and sheets, *Environ. Sci. Technol.* **56**, 8114 (2022).
- [42] A. G. López, R. G. Najjar, M. A. M. Friedrichs, M. A. Hickner, and D. H. Wardrop, Estuaries as filters for riverine microplastics: Simulations in a large, Coastal-Plain Estuary, *Front. Mar. Sci.* **8**, 715924 (2021).
- [43] V. S. Koutnik, J. Leonard, S. Alkidim, F. J. DePrima, S. Ravi, E. M. V. Hoek, and S. K. Mohanty, Distribution of microplastics in soil and freshwater environments: Global analysis and framework for transport modeling, *Environ. Pollut.* **274**, 116552 (2021).
- [44] P. Ern, F. Risso, D. Fabre, and J. Magnaudet, Wake-induced oscillatory paths of bodies freely rising or falling in fluids, *Annu. Rev. Fluid Mech.* **44**, 97 (2011).
- [45] J. Dušek, Path instabilities of axisymmetric bodies falling or rising under the action of gravity and hydrodynamic forces in a Newtonian fluid, *Particles in Flows* (Birkhäuser, Cham, 2017), p. 397.
- [46] P. C. Fernandes, P. Ern, F. Risso, and J. Magnaudet, Dynamics of axisymmetric bodies rising along a zigzag path, *J. Fluid Mech.* **606**, 209 (2008).
- [47] W. Fornari, M. N. Ardekani, and L. Brandt, Clustering and increased settling speed of oblate particles at finite Reynolds number, *J. Fluid Mech.* **848**, 696 (2018).
- [48] N. R. Challabotla, L. Zhao, and H. I. Andersson, Orientation and rotation of inertial disk particles in wall turbulence, *J. Fluid Mech.* **766**, R2 (2015).
- [49] C. Marchioli, M. Fantoni, and A. Soldati, Orientation, distribution, and deposition of elongated, inertial fibers in turbulent channel flow, *Phys. Fluids* **22**, 033301 (2010).
- [50] H. I. Andersson and F. Jiang, Forces and torques on a prolate spheroid: Low-Reynolds-number and attack angle effects, *Acta Mech.* **230**, 431 (2019).

- [51] S. J. Xu, W. G. Zhang, L. Gan, M. G. Li, and Y. Zhou, Experimental study of flow around polygonal cylinders, *J. Fluid Mech.* **812**, 251 (2017).
- [52] N. Pujara, T. B. Oehmke, A. D. Bordoloi, and E. A. Variano, Rotations of large inertial cubes, cuboids, cones, and cylinders in turbulence, *Phys. Rev. Fluids* **3**, 054605 (2018).
- [53] E. Kanso, L. Heisinger, and P. Newton, Coins falling in water, *J. Fluid Mech.* **742**, 243 (2014).
- [54] M. L. Byron, Y. Tao, I. A. Houghton, and E. A. Variano, Slip velocity of large low-aspect-ratio cylinders in homogeneous isotropic turbulence, *Int. J. Multiphase Flow* **121**, 103120 (2019).
- [55] P. C. Fernandes, F. D. Risso, P. Ern, and J. Magnaudet, Oscillatory motion and wake instability of freely rising axisymmetric bodies, *J. Fluid Mech.* **573**, 479 (2007).
- [56] E. K. Marchildon, A. Clamen, and W. H. Gauvin, Drag and oscillatory motion of freely falling cylindrical particles, *Can. J. Chem. Eng.* **42**, 178 (1964).
- [57] R. Natarajan and A. Acrivos, The instability of the steady flow past spheres and disks, *J. Fluid Mech.* **254**, 323 (1993).
- [58] R. H. Magarvey and R. L. Bishop, Transition ranges for three-dimensional wakes, *Can. J. Phys.* **39**, 1418 (1961).
- [59] F. Auguste, D. Fabre, and J. Magnaudet, Bifurcations in the wake of a thick circular disk, *Theor. Comput. Fluid Dyn.* **24**, 305 (2010).
- [60] O. Inoue and A. Sakuragi, Vortex shedding from a circular cylinder of finite length at low Reynolds numbers, *Phys. Fluids* **20**, 033601 (2008).
- [61] C. H. K. Williamson, Vortex dynamics in the cylinder wake, *Annu. Rev. Fluid Mech.* **28**, 477 (1996).
- [62] J. Magnaudet and G. Mougin, Wake instability of a fixed spheroidal bubble, *J. Fluid Mech.* **572**, 311 (2007).
- [63] M. Jenny, J. Ducek, and G. Bouchet, Instabilities and transition of a sphere falling or ascending freely in a Newtonian fluid, *J. Fluid Mech.* **508**, 201 (2004).
- [64] B. Chung, M. Cohrs, W. Ernst, G. P. Galdi, and A. Vaidya, Wake–cylinder interactions of a hinged cylinder at low and intermediate Reynolds numbers, *Arch. Appl. Mech.* **86**, 627 (2015).
- [65] C. Toupoint, P. Ern, and V. Roig, Kinematics and wake of freely falling cylinders at moderate Reynolds numbers, *J. Fluid Mech.* **866**, 82 (2019).
- [66] A. B. Burd and G. A. Jackson, Particle aggregation, *Ann. Rev. Marine Sci.* **1**, 65 (2009).
- [67] C. P. Johnson, X. Li, and B. E. Logan, Settling velocities of fractal aggregates, *Environ. Sci. Technol.* **30**, 1911 (1996).
- [68] P. Tang and J. A. Raper, Modelling the settling behaviour of fractal aggregates—A review, *Powder Technol.* **123**, 114 (2002).
- [69] O. S. Alimi, J. Farner Budarz, L. M. Hernandez, and N. Tufenkji, Microplastics and nanoplastics in aquatic environments: Aggregation, deposition, and enhanced contaminant transport, *Environ. Sci. Technol.* **52**, 1704 (2018).
- [70] Y. Cui, J. Ravnik, P. Steinmann, and M. Hriberšek, Settling characteristics of nonspherical porous sludge flocs with nonhomogeneous mass distribution, *Water Res.* **158**, 159 (2019).
- [71] S. Yasseri, Experiment of free-falling cylinders in water, *Underwater Technol.* **32**, 177 (2014).
- [72] A. V. Abelev, P. J. Valent, and K. T. Holland, Behavior of a large cylinder in free-fall through water, *IEEE J. Oceanic Eng.* **32**, 10 (2007).
- [73] J. Lan, P. Fleischer, C. W. Fan, P. C. Chu, and A. F. Gilles, Hydrodynamics of falling cylinder in water column, *Advances in Fluid Mechanics*, Vol. 4 (WIT Press, 2002), p. 163.
- [74] M. Byron and E. A. Variano, Refractive-index-matched hydrogel materials for measuring flow-structure interactions, *Exp. Fluids* **54**, 1456 (2013).
- [75] N. Pujara, M. A. R. Koehl, and E. A. Variano, Rotations and accumulation of ellipsoidal microswimmers in isotropic turbulence, *J. Fluid Mech.* **838**, 356 (2017).
- [76] Y. Man and E. Kanso, Multisynchrony in active microfilaments, *Phys. Rev. Lett.* **125**, 148101 (2020).
- [77] A. D. Bordoloi and E. Variano, Rotational kinematics of large cylindrical particles in turbulence, *J. Fluid Mech.* **815**, 199 (2017).

- [78] See Supplemental Material at <http://link.aps.org/supplemental/10.1103/PhysRevFluids.9.070501> for a description of particle drag coefficient calculations, hydrogel density measurements, three-dimensional imaging calibration, and descriptions of supplemental videos.
- [79] Ronald J. Gibbs, Martin D. Matthews, and David A. Link, The relationship between sphere size and settling velocity, *J. Sediment. Petrol.* **41**, 7 (2008).
- [80] P. P. Brown and D. F. Lawler, Sphere drag and settling velocity revisited, *J. Environ. Eng.* **129**, 222 (2003).
- [81] J. P. le Roux, Settling velocity of spheres: A new approach, *Sediment. Geol.* **81**, 11 (1992).
- [82] A. ten Cate, C. H. Nieuwstad, J. J. Derksen, and H. E. A. Van den Akker, Particle imaging velocimetry experiments and Lattice-Boltzmann simulations on a single sphere settling under gravity, *Phys. Fluids* **14**, 4012 (2002).
- [83] R. Clift and W. H. Gauvin, Motion of entrained particles in gas streams, *Can. J. Chem. Eng.* **49**, 439 (1971).
- [84] L. Schiller and A. Z. Naumann, Über die grundlegenden Berechnungen bei der Schwerkraftaufbereitung, *Z. Vereines Deutscher Inge* **77**, 318 (1933).
- [85] R. P. Chhabra, L. Agarwal, and N. K. Sinha, Drag on non-spherical particles: An evaluation of available methods, *Powder Technol.* **101**, 288 (1999).
- [86] S. Tran-Cong, M. Gay, and E. E. Michaelides, Drag coefficients of irregularly shaped particles, *Powder Technol.* **139**, 21 (2004).
- [87] T. L. Hedrick, Software techniques for two- and three-dimensional kinematic measurements of biological and biomimetic systems, *Bioinspiration Biomimetics* **3**, 034001 (2008).
- [88] Y. I. Abdel-Aziz and H. M. Karara, Direct linear transformation from comparator coordinates into object space coordinates in close-range photogrammetry, *Photogramm. Eng. Remote Sens.* **81**, 103 (2015).
- [89] W. Thielicke and E. J. Stamhuis, PIVLAB—Towards user-friendly, affordable and accurate digital particle image velocimetry in MATLAB, *J. Open Res. Softw.* **2**, e30 (2014).
- [90] D. Garcia, Robust smoothing of gridded data in one and higher dimensions with missing values, *Comput. Stat. Data Anal.* **54**, 1167 (2010).
- [91] J. D. Eldredge and A. R. Jones, Leading-edge vortices: Mechanics and modeling, *Annu. Rev. Fluid Mech.* **51**, 75 (2019).
- [92] P. C. Fernandes, P. Ern, F. Risso, and J. Magnaudet, On the zigzag dynamics of freely moving axisymmetric bodies, *Phys. Fluids* **17**, 098107 (2005).
- [93] P. Ern, P. C. Fernandes, F. Risso, and J. Magnaudet, Evolution of wake structure and wake-induced loads along the path of freely rising axisymmetric bodies, *Phys. Fluids* **19**, 113302 (2007).
- [94] V. Mathai, X. Zhu, C. Sun, and D. Lohse, Mass and moment of inertia govern the transition in the dynamics and wakes of freely rising and falling cylinders, *Phys. Rev. Lett.* **119**, 054501 (2017).